(Received 22 November 2023, Accepted 3 January 2024, Scheduled 15 January 2024)

Realization of a Second-Order Wide-Stopband Substrate-Integrated Waveguide Filter Using the Weakest Electric Field Method and DGS Structure

Yuxin Fang, Xiaohei Yan*, Yixian Wang, and Shengbing Zhang

School of Mathematics and Electronic Information Engineering, Guangxi Minzu Normal University, Chongzuo 532200, China

ABSTRACT: To increase the stopband width of the filter, a second-order wide-stopband substrate-integrated waveguide filter is suggested. This filter is designed by utilizing a DGS structure and the weakest electric field approach. To suppress the modes, the filter sets the inner and outer coupling windows at the modes' weakest electric fields (TE_{120}/TE_{210}, TE_{220}). Additionally, a new nested U-shaped DGS structure is implemented to suppress the TE_{130} mode, hence expanding the stopband width of the filter. The filter has been processed and measured, and the findings indicate a 4.5 GHz center frequency, a -3 dB bandwidth of 240 MHz, a relative bandwidth of 5.3%, an insertion loss of -1.2 dB in the passband, and a -22 dB stopband, which can be extended up to 9.4 GHz (i.e., 2.1 times the center frequency). The simulated and measured results demonstrate good alignment. Compared to other SIW filters, the current filter achieves a wider stopband while using fewer orders and implementing a straightforward design method, providing potential value for applications.

1. INTRODUCTION

Substrate integrated waveguide (SIW) offers several advantages, including low cost, low loss, small size, high-quality factor, and easy integration, making it widely used in designing different microwave devices, including filters, couplers, duplexers, and antennas [1–5]. However, the multimode resonance characteristics of SIW resonant cavities lead to limited stopband width in filters designed using them.

To enhance the stopband width of filters, researchers have explored multiple techniques to widen the stopband of SIW filters [6–15]. One method, presented in [6], involves cascading low-pass filters to extend the filter's stopband width. However, this approach increases the circuit size and loss, making it unfavorable for integration into communication systems. In previous studies [7], researchers utilized various shapes of SIW cavities to reduce harmonic coupling and enhance the filter's out-of-band rejection performance. However, this technique resulted in an increase in filter design complexity. Another study [8] positioned the external or internal coupling window at the weakest electric field of a particular mode, but it only proved effective in suppressing the TE_{120} high-order mode. Ref. [9] corrects the orthogonality of modes by adjusting the coupling at the port, which expands the filter's stopband. However, the extension of the stopband is still narrow. Ref. [10] selects a particular cavity size to create a first harmonic passband located away from the primary mode passband and arranges the higher harmonics coupling in a staggered pattern. This approach achieves a broader stopband for the filter. However, the method relies on a cavity with a specific aspect ratio, limiting its applicability. In Ref. [11], it is possible to achieve a higher level of out-of-band rejection through the introduction of transmission zeros for harmonic suppression. However, this method has limited capability, which restricts the stopband width expansion. In contrast, researchers in [12] used a multilayer coupling structure to design a wide stopband filter, but it only produced a stopband of 2 times of the center frequency, and the extension range was somewhat insufficient. Ref. [13] proposes a wide-stopband filter based on an integrated substrate gap waveguide. However, it uses resonant cavities with different dimensions, which can lead to wasted space when being integrated into a communication system. In contrast, [14] uses electromagnetic hybrid coupling to design a multilayer structured wide-bandstop filter, which reduces planar dimensions to some extent but has a large insertion loss. Ref. [15] designs a wide-stopband filter with a single-layer structure using mixed quarter- and one-eighth-mode cavities. However, the filter's shape is highly specific, which limits its potential applications.

The filters discussed in previous literature fail to achieve a comprehensive balance among stopband width, filter structure, and design method. Hence, this paper proposes a single-layer, second-order, wide-stopband SIW bandpass filter. Firstly, the suppression of high-order modes (TE_{120}/TE_{210}, TE_{220}) is achieved by placing the inner and outer coupling windows at the weakest electric field position. Subsequently, a new defected ground structure (DGS) structure with a nested U-shape is proposed, and it is used to suppress the TE_{130} mode by etching it on metallic ground, thereby extending the filter's stopband width. The filter was processed and tested, and the experimental results confirmed the feasibility of the proposed design method, as they exhibited high agreement with the simulated and measured results.

* Corresponding author: Xiaohei Yan (yanxiaohei@gxnun.edu.cn).

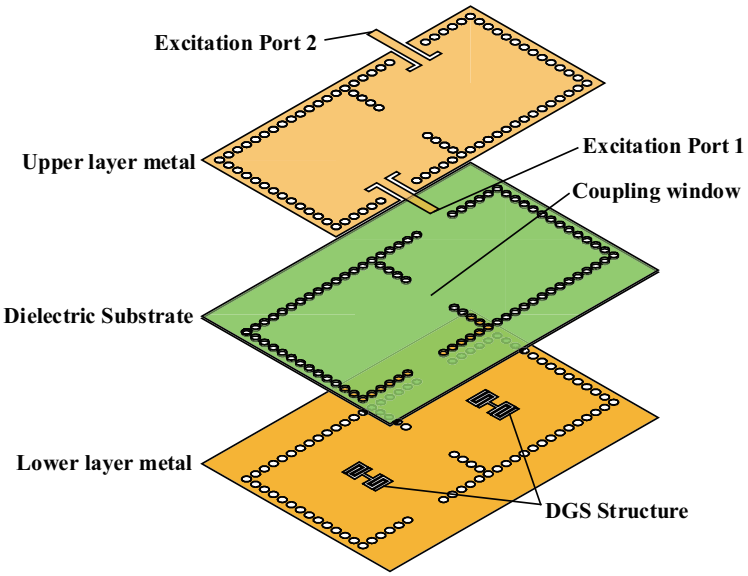

FIGURE 1. Structure of the filter.

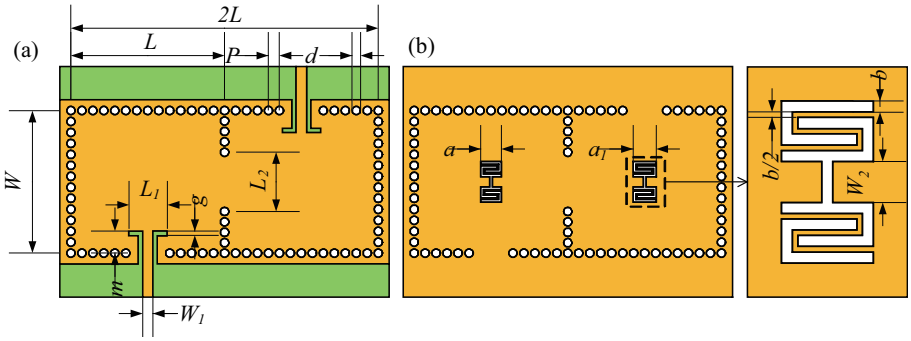

FIGURE 2. Dimensional drawings of the metal layers. (a) Upper layer metal; (b) Lower layer metal.

2. FILTER STRUCTURE

This design utilizes a substrate-integrated waveguide cavity structure with a single layer. Figure 1 depicts its 3D structure which consists of two metal layers and one dielectric layer. The dielectric layer's material is ZYF300CA-P, with a relative permittivity of 3, loss tangent of 0.0018, and thickness of 0.762 mm. The rectangular substrate-integrated waveguide cavity comprises two resonant cavities and operates in TE_{110} mode. The two resonant cavities are coupled through a window in the middle of the common edge. Both input and output ports are situated in the sidewalls of the resonant cavities and are structured with coplanar waveguides to achieve energy coupling between the source/load and filter. Two defected ground structure (DGS) units of varying sizes have been etched into the lower metal layer of both resonance cavities. The DGS units feature a nested U-shape structure, which introduces transmission zeros at specific frequency points that require suppression, thereby enhancing the filter's blocking performance and expanding its blocking bandwidth. Refer to Figure 2 for an illustration of the metal layer shape implemented in the filter. After optimizing the simulation using HFSS simulation software, Table 1 displays the ultimate structural parameters of the filter. beneath:

TABLE 1. Filter structural parameters (unit: mm).

$L = 56$	$P = 2$	$d = 1.5$	$W = 26$
$m = 4$	$g = 0.8$	$L_1 = 7$	$W_1 = 1.88$
$L_2 = 10.8$	$a = 3.8$	$a_1 = 4.2$	$b = 0.5$
$W_2 = 1.88$			

3. FILTER DESIGN AND PRINCIPLE ANALYSIS

3.1. SIW Resonant Cavity Theory

The SIW features an inventive waveguide-style design that boasts electromagnetic field transmission characteristics akin to those of a rectangular waveguide. Periodically spaced metallized vias in the sidewalls of the SIW interrupt the current component in the direction of propagation along the longitudinal direction, leading to a radiation effect. Consequently, the transmission of the transverse magnetic wave TM_{mn0} mode is

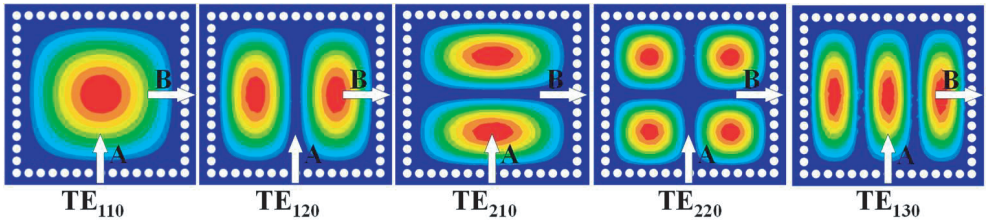

FIGURE 3. Electric field strength distribution of some modes in the SIW resonant cavity.

not viable in the SIW. On the other hand, the TE_{mn0} mode of the transverse electric wave only has a magnetic field component in the direction of longitudinal propagation and lacks an electric field component. Thus, the SIW rectangular resonant cavity can solely transfer TE_{mn0} modes and has the resonant frequency equation displayed

$$f_{TEmn0} = \frac{c_0}{2\sqrt{\varepsilon_r}}\sqrt{\left(\frac{m}{W_{eff}}\right)^2 + \left(\frac{n}{L_{eff}}\right)^2} \tag{1}$$

where c_0 is the speed of light in vacuum; ε_r is the dielectric constant of the dielectric substrate; m, n are the number of modes along the width and length directions, respectively; w_{eff} and l_{eff} are the equivalent width and length of the SIW structure, which are defined as follows:

$$W_{eff} = W - \frac{d^2}{0.95p}, \quad L_{eff} = L - \frac{d^2}{0.95p} \tag{2}$$

wherein the center distance between two rows of circular holes on the wide side of the cavity is denoted by W; the center distance between two columns of circular holes on the long side of the cavity is denoted by L; the diameter of the circular holes is denoted by d; and the circumcentric distance between adjacent circular holes is denoted by p.

In this design, the filter operates in the 5G Sub-6G band. Therefore, the initial resonant frequency of the TE_{110} mode is assumed to be 4.5 GHz by setting $P = 2$ mm and $d = 1.5$ mm. The cavity dimensions can then be initially calculated following Equations (1) and (2):

$$W = 26\,\text{mm}, \quad L = 28\,\text{mm} \tag{3}$$

SIW resonators have a large number of resonant modes, which can limit the filter stopband. Filters designed with SIW resonators have harmonic passbands closer to the dominant mode passband than other types of microwave filters. To broaden the stopband range of SIW filters, it is crucial to suppress as many high-order modes as possible. In the rectangular resonant cavity with SIW, the modes are ordered as TE_{110}, TE_{120}/TE_{210}, TE_{220}, and TE_{130}/TE_{310}, in increasing frequency. To achieve wide stopband performance in the SIW filter, it is necessary to suppress high-order modes according to their resonant frequencies, from low to high.

3.2. Analysis of Suppression Methods for Mode

This design utilizes a technique of placing external excitation ports and internal coupling windows at the weakest electric fields of particular modes within the SIW resonant cavity in order to eliminate resonant coupling of specific modes. Notably, Figure 3 illustrates that the external excitation port and the internal coupling window are all located at the center of the sidewalls, specifically at points A and B as indicated in Figure 3. This method ensures not only optimal magnetic coupling of the TE_{110} mode but also efficient suppression of the TE_{120}/TE_{210} and TE_{220} modes. However, it is ineffective in suppressing the TE_{130}/TE_{310} modes, and alternative approaches are necessary to achieve such suppression.

DGS is a recent microwave device design that employs a defective structure etched on the metal ground of a microwave device with bandstop characteristics. By etching a DGS structure on the metal ground of the substrate-integrated waveguide cavity, the device can suppress the signal at a specific frequency point. This leads to improvements in the filter's stopband performance and extends the filter's stopband width.

In this study, an original nested U-shaped DGS structure is suggested in the manner demonstrated in Figure 2. In comparison to the evaluated dumbbell-type DGS structure, the nested U-shaped DGS structure heightens the etching paths, hence enhancing the equivalent capacitance and inductance while consuming less space than the dumbbell-type DGS structure with the same resistive band center frequency. Meanwhile, to minimize the effect of dimension on the DGS structure, the proposed nested U-shaped DGS structure can be determined with just three dimensions (a, b, and W_2). To study how a change in dimensions affects the bandstop characteristics of the DGS structure, we created the extracted model displayed in Figure 4. We kept b and W_2 constant at 0.5 mm and 1.88 mm, respectively, and obtained bandstop characteristic curves of the DGS structure through simulation, as seen in Figure 5. The DGS structure demonstrates bandstop characteristics. As the value of a increases, the center frequency of the resistive band shifts towards the low-frequency direction. This occurs because an increase in the value of a results in increased equivalent inductance and capacitance of the DGS structure.

By merging the above two rejection techniques, a broad stopband filter can be created to meet the necessary requirements.

3.3. Equivalent Circuit of the Filter

The filter's equivalent circuit representation can be found in Figure 6. Two resonant cavities in the substrate-integrated waveguide, both operating in TE_{110} mode, can be viewed as two LC parallel resonant circuits that work as a bandpass. Two DGS structures etched on the metal ground can be seen as two

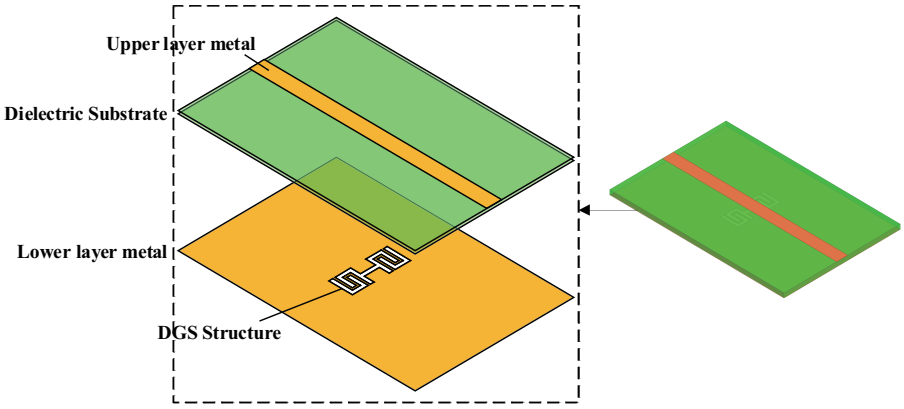

FIGURE 4. Extracted model of resistive band properties of DGS structure.

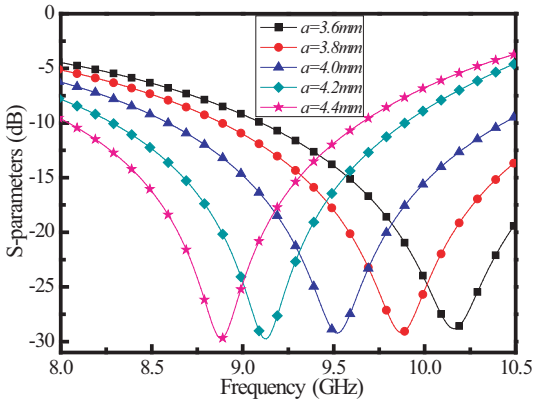

FIGURE 5. Variation of bandstop characteristics of DGS structure with a dimension.

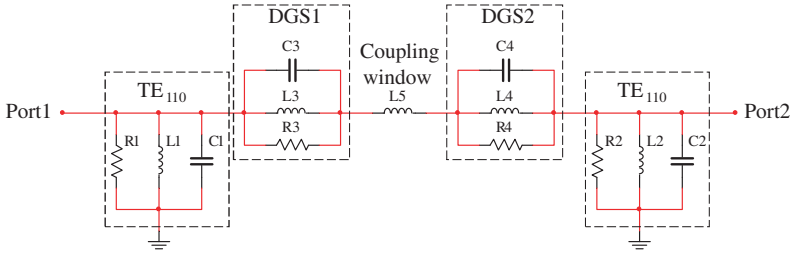

FIGURE 6. Equivalent circuit of the filter.

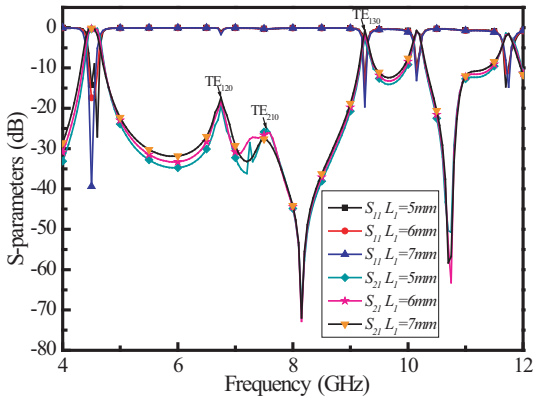

FIGURE 7. S-parameter curves of the filter without DGS loading.

LC parallel resonant circuits connected in series to the resonant cavities, working as a bandstop. The coupling window connecting the two resonant cavities can be considered an inductance, which allows for the energy exchange between the two cavities. This allows the filter to facilitate the transmission of signals within a specific frequency range while suppressing signals within another specific frequency range. Furthermore, by adjusting the dimensions of the DGS structure, the filter can have its stopband characteristics adjusted to achieve a wide stopband.

4. RESULTS AND ANALYSIS

4.1. Simulation Results of the Filter without DGS Loading

The S-parameters of the filter without DGS loading are simulated in Figure 7. The data show that only TE_{120}/TE_{210} and TE_{220} modes can be achieved through the weakest electric field method when suppressing high-order modes. No suppression effect is observed on the TE_{130} mode. When the value of L_1 is reduced from 7 mm to 5 mm, the insertion loss at the frequency

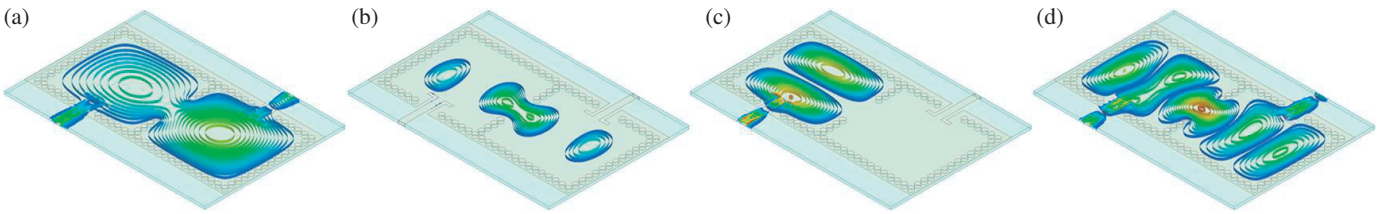

FIGURE 8. Electric field strength distribution at different frequencies for the filter without DGS loading. (a) 4.5 GHz; (b) 6.75 GHz; (c) 7.5 GHz; (d) 9.25 GHz.

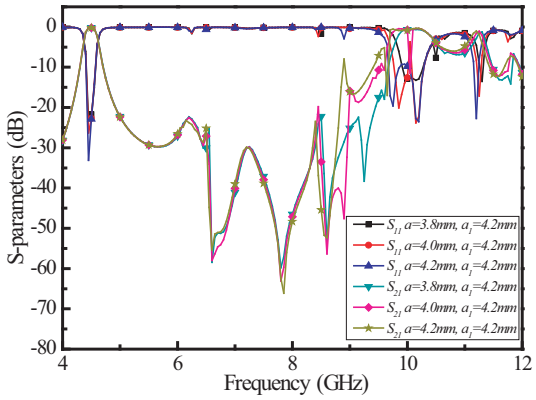

FIGURE 9. S-parameter curves of filters with different a/a_1 dimensions.

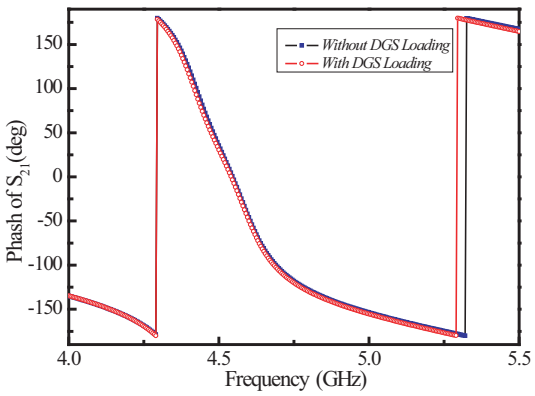

FIGURE 10. The phase characteristic curves of the S_{21} parameter.

of the TE_{130} mode changes from -0.64 dB to -2.88 dB, but the insertion loss in the passband of the filter also changes from -0.4 dB to -0.8 dB, and the return loss changes from -31 dB to -9 dB. Therefore, it is possible to enhance the rejection of the TE_{130} mode through altering the dimensions of the input/output ports by reducing L_1; however, it only yields a minor improvement and adversely affects the filter's passband performance. Considering all relevant factors, we aim to ensure the filter's passband performance while suppressing the TE_{130} mode through the utilization of a DGS structure etched on the metal ground. This technique effectively extends the stopband width of the filter.

The electric field strength distribution of the filter without DGS loading at different frequencies is shown in Figure 8. Observably, the filter smoothly allows the signal to pass at the passband's center frequency of 4.5 GHz. Additionally, the signal is effectively suppressed at the frequencies of TE_{120}/TE_{210} modes (6.75 GHz and 7.5 GHz). At a frequency of 9.25 GHz in TE_{130} mode, the signal output is robust. This outcome aligns with the findings reflected in the S-parameters of the filter.

4.2. Simulation Results of the Filter with DGS Loading

The DGS structure is an etched defect pattern located on the metal ground surface of the substrate-integrated waveguide cavity, which possesses a bandstop characteristic. By manipulating the size of the structure, a transmission zero can be introduced at a specific frequency on the filter stopband. This results in the suppression of corresponding high-order modes and the expansion of the stopband width of the filter. In this design, a DGS structure is etched in the center of the metal ground of each of the two resonant cavities for the suppression of TE_{130} high-order mode, and the suppression effect on TE_{130} mode is mainly adjusted by adjusting the a/a_1 dimensions of the DGS structure. Figure 9 provides the S-parameter curves of the filter with varying a/a_1 dimensions. The introduction of two transmission zeros near the frequency of the TE_{130} mode is facilitated by the two DGS structures with different dimensions. The TE_{130} high-order mode is better suppressed when $a = 3.8$ mm, $a_1 = 4.2$ mm.

Figure 10 displays the phase characteristic curves of the S_{21} parameter of the filter. It is evident that the loading of the DGS structure has a minimal impact on the phase characteristic of the filter. Additionally, the linearity of the phase characteristic of the filter is superior in the passband. Figure 11 displays the group delay curves of the filter. It is evident that the DGS structure loading has a negligible impact on the group delay of the filter. Moreover, the group delay of the filter is less than 2.7 ns in the passband, and the maximum group delay variation is only 0.7 ns.

Figure 12 displays the electric field strength distribution at various frequencies for the DGS-loaded filter. The signal is minimally impacted by the DGS structure and flows through the filter smoothly at the center frequency of the filter passband, 4.5 GHz. However, at the frequencies of TE_{120}/TE_{210} modes (6.5 GHz and 7.25 GHz), the signal experiences better suppression. At a frequency of 9.15 GHz in TE_{130} mode, the DGS structure can successfully suppress the signal, preventing it from passing through the filter. This aligns with the S-parameter results displayed in the filter.

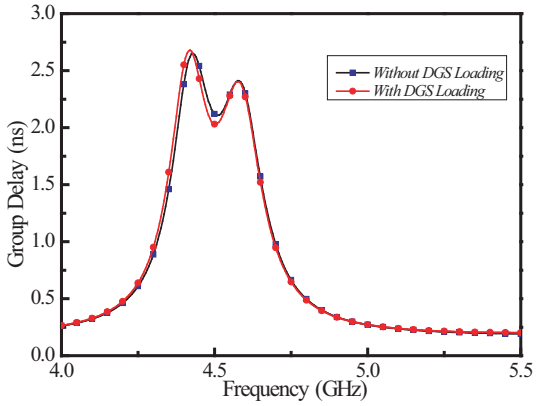

FIGURE 11. The group delay curves of the filter.

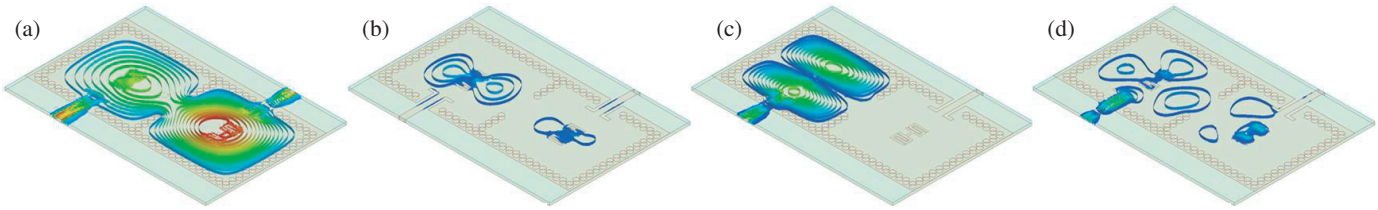

FIGURE 12. Electric field strength distribution at different frequencies for the filter with DGS loading. (a) 4.5 GHz; (b) 6.5 GHz; (c) 7.25 GHz; (d) 9.15 GHz.

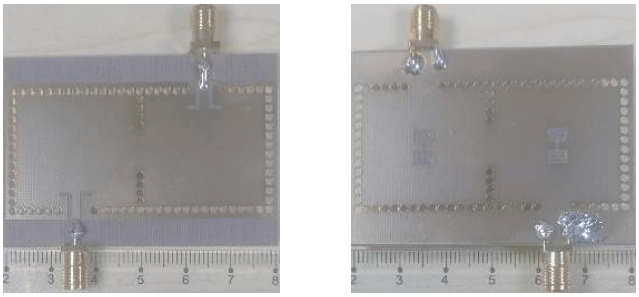

FIGURE 13. Filter object.

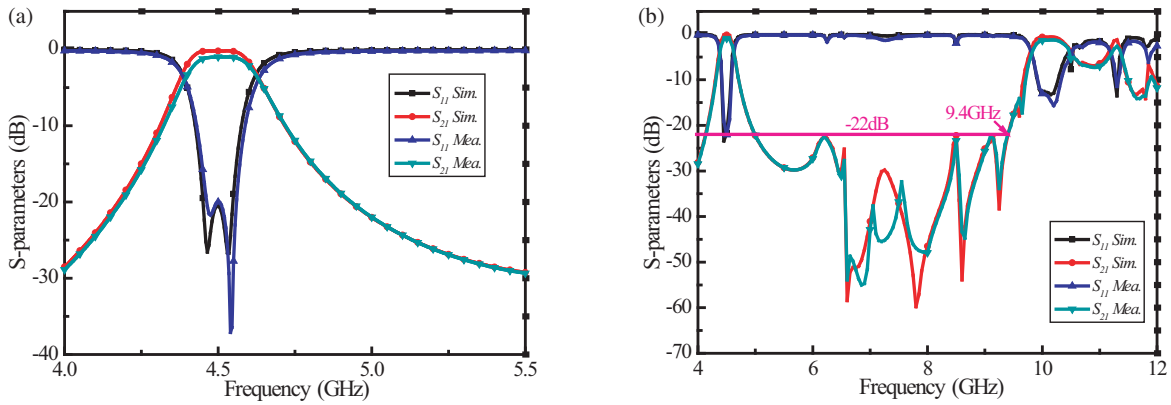

FIGURE 14. Simulated and measured S-parameter curves of the filter. (a) Passband transmission response of the filter; (b) Stopband transmission response of the filter.

TABLE 2. Comparison with similar filters in the literature.

Refs.	F_0 (GHz)	Relative Bandwidth (%)	Filter Order	Insertion Loss (dB)	size (λ_g^2)	Resistance Bandwidth
[9]	15	4	5	2.3	3	55 dB/1.96f_0
[10]	10	1.51	3	2.91	1.86	25 dB/2.1f_0
[11]	20	2.75	4	2.78	\	20 dB/1.90f_0
[12]	13	4.55	2	1.5	0.46	20 dB/2.39f_0
[13]	21.1	4.16	2	\	\	20 dB/2.13f_0
[14]	9.55	2.95	2	2.62	3.56	20 dB/2.1f_0
[15]	8	8.12	2	0.9	0.15	17 dB/2.1f_0
This work	4.5	5.3	2	1.2	1.2	22 dB/2.1f_0

4.3. Comparison of Simulation and Test Results

Based on dimensions in Table 1, the physical filter was processed using PCB process, and the physical filter is shown in Figure 13. In order to conduct the physical test, it is essential to attach SMA-KHD coaxial connectors to the input and output ports of the filter and link them to an Agilent E8363C model network vector analyzer for measurement. The measured and simulated S-parameter curves display a consistent overall trend for the filter, as depicted in Figure 14. The simulation shows that the center frequency of the filter is 4.5 GHz; the -3 dB bandwidth is 240 MHz; the relative bandwidth is 5.3%; the insertion loss in the passband is about -0.4 dB; and the -22 dB stopband can be extended to 9.4 GHz (i.e., 2.1 times the center frequency). However, the actual measurement recorded an insertion loss that is 0.8 dB lower than the simulated value. The disparity between the measured and simulated insertion losses is primarily due to processing errors, dielectric losses, and conversion structure losses.

Table 2 provides a comparison between the proposed filter in this paper and the SIW filters proposed in references. The proposed filter in this paper outperforms the others in terms of order, insertion loss, relative bandwidth, and blocking bandwidth, and the design methodology used is simple and easy to implement.

5. CONCLUSION

To broaden the stopband width of the filter, this research introduces a second-order wide-stopband substrate-integrated waveguide filter, which is implemented by utilizing the weakest electric field method and DGS structure. To attain the mode suppression effect, this filter arranges the inner and outer coupling windows at the weakest electric field of the modes (TE_{120}/TE_{210}, TE_{220}). Meanwhile, this paper introduces a novel nested U-shaped DGS structure for the suppression of TE_{130} mode to further extend the stopband width of the filter. The simulated and measured outcomes exhibit that the filter owns a center frequency of 4.5 GHz, a -3 dB bandwidth of 240 MHz, a relative bandwidth of 5.3%, an insertion loss of -1.2 dB in the passband, and a -22 dB stopband, which can be expanded to 9.4 GHz (i.e., 2.1 times the center frequency). Compared to other SIW filters, the present filter achieves a relatively wide stopband with fewer orders and a simplified design. This filter holds promise for various applications.

ACKNOWLEDGEMENT

This work is supported by the Guangxi University Student Innovation and Entrepreneurship Training Program Project (No. 202310604002), and the Chongzuo Science and Technology Program Project (No. 2023ZC025654), and the School-level Research Project of Guangxi Minzu Normal University (No. 2022SP007).

REFERENCES

[1] Bozzi, M., A. Georgiadis, and K. Wu, "Review of substrate-integrated waveguide circuits and antennas," *IET Microwaves, Antennas & Propagation*, Vol. 5, No. 8, 909–920, Jun. 2011.

[2] Chen, X.-P. and K. Wu, "Substrate integrated waveguide filter: Basic design rules and fundamental structure features," *IEEE Microwave Magazine*, Vol. 15, No. 5, 108–116, Jul.–Aug. 2014.

[3] Moscato, S., C. Tomassoni, M. Bozzi, and L. Perregrini, "Quarter-mode cavity filters in substrate integrated waveguide technology," *IEEE Transactions on Microwave Theory and Techniques*, Vol. 64, No. 8, 2538–2547, Aug. 2016.

[4] Jones, T. R. and M. Daneshmand, "Miniaturized folded ridged half-mode and quarter-mode substrate integrated waveguides for filter design," *IEEE Transactions on Microwave Theory and Techniques*, Vol. 67, No. 8, 3414–3426, Aug. 2019.

[5] Liu, Q., D. Zhang, M. Tang, H. Deng, and D. Zhou, "A class of box-like bandpass filters with wide stopband based on new dual-mode rectangular SIW cavities," *IEEE Transactions on Microwave Theory and Techniques*, Vol. 69, No. 1, 101–110, Jan. 2021.

[6] Yun, T.-S., H. Nam, J.-Y. Kim *et al.*, "Harmonics suppressed substrate-integrated waveguide filter with integration of low-pass filter," *Microwave and Optical Technology Letters*, Vol. 50, No. 2, 447–450, 2008.

[7] Zhou, K., C. Zhou, and W. Wu, "Substrate integrated waveguide dual-band filter with wide-stopband performance," *Electronics Letters*, Vol. 53, No. 16, 1121–1123, Aug. 2017.

[8] Chu, P., K.-L. Zheng, F. Xu, and K. Wu, "Substrate integrated waveguide resonator with harmonic suppression," *Electronics Letters*, Vol. 54, No. 24, 1388–1389, Nov. 2018.

[9] Chu, P., L. Guo, L. Zhang, F. Xu, W. Hong, and K. Wu, "Wide stopband substrate integrated waveguide filter implemented by orthogonal ports' offset," *IEEE Transactions on Microwave Theory and Techniques*, Vol. 68, No. 3, 964–970, Mar. 2020.

[10] Zhou, K., C.-X. Zhou, and W. Wu, "Resonance characteristics of substrate-integrated rectangular cavity and their applications to dual-band and wide-stopband bandpass filters design," *IEEE Transactions on Microwave Theory and Techniques*, Vol. 65, No. 5, 1511–1524, May 2017.

[11] Zhu, F., W. Hong, J. X. Chen, and K. Wu, "Wide stopband substrate integrated waveguide filter using corner cavities," *Electronics Letters*, Vol. 49, No. 1, 50–52, Jan. 2013.

[12] Jia, D., Q. Feng, Q. Xiang, and K. Wu, "Multilayer substrate integrated waveguide (SIW) filters with higher-order mode suppression," *IEEE Microwave and Wireless Components Letters*, Vol. 26, No. 9, 678–680, Sep. 2016.

[13] Yang, H., D. Shen, L. Li, Q. Kang, and K. Kai, "Integrated substrate gap waveguide bandpass filter with wide stopband," in *2023 16th UK-Europe-China Workshop on Millimetre Waves and Terahertz Technologies (UCMMT)*, 1–3, Guangzhou, China, 2023.

[14] Su, Z. L., B. W. Xu, S. Y. Zheng, H. W. Liu, and Y. L. Long, "High-isolation and wide-stopband SIW diplexer using mixed electric and magnetic coupling," *IEEE Transactions on Circuits and Systems II: Express Briefs*, Vol. 67, No. 1, 32–36, Jan. 2020.

[15] Kim, P. and Y. Jeong, "Compact and wide stopband substrate integrated waveguide bandpass filter using mixed quarter-and one-eighth modes cavities," *IEEE Microwave and Wireless Components Letters*, Vol. 30, No. 1, 16–19, Jan. 2020.